



OPEN ACCESS

EDITED BY

Sung Bae Kim,
National Institute of Advanced Industrial
Science and Technology (AIST), Japan

REVIEWED BY

Melissa Sprachman,
Draper Laboratory, United States
Jyothi Sistla,
Stony Brook University, United States

*CORRESPONDENCE

Mai Yamagishi,
✉ myamagishi@lcd.co.jp
Yoshitaka Shirasaki,
✉ shirasaki@g.ecc.u-tokyo.ac.jp

RECEIVED 30 April 2024

ACCEPTED 18 November 2024

PUBLISHED 21 January 2025

CITATION

Yamagishi M, Hori Y, Suzuki N, Peng Y, Harada Y,
Funatsu T, Ohara O and Shirasaki Y (2025)
Evaluation of the microenvironment formed
by interferon- β .
Front. Chem. Biol. 3:1425571.
doi: 10.3389/fchbi.2024.1425571

COPYRIGHT

© 2025 Yamagishi, Hori, Suzuki, Peng, Harada,
Funatsu, Ohara and Shirasaki. This is an open-
access article distributed under the terms of the
[Creative Commons Attribution License \(CC BY\)](https://creativecommons.org/licenses/by/4.0/).
The use, distribution or reproduction in other
forums is permitted, provided the original
author(s) and the copyright owner(s) are
credited and that the original publication in this
journal is cited, in accordance with accepted
academic practice. No use, distribution or
reproduction is permitted which does not
comply with these terms.

Evaluation of the microenvironment formed by interferon- β

Mai Yamagishi^{1,2*}, Yutaka Hori³, Nobutake Suzuki^{1,2}, Yu Peng^{4,5},
Yoshie Harada⁴, Takashi Funatsu¹, Osamu Ohara⁶ and
Yoshitaka Shirasaki^{1,7*}

¹Graduate School of Pharmaceutical Sciences, The University of Tokyo, Tokyo, Japan, ²Live Cell Diagnosis, Ltd., Saitama, Japan, ³Department of Applied Physics and Physico-informatics, Faculty of Science and Technology, Keio University, Yokohama, Kanagawa, Japan, ⁴Institute for Protein Research, Osaka University, Osaka, Japan, ⁵Graduate School of Science, Osaka University, Osaka, Japan, ⁶Department of Applied Genomics, Kazusa DNA Research Institute, Chiba, Japan, ⁷Research Center for Advanced Science and Technology, The University of Tokyo, Tokyo, Japan

Heterogeneity in the cellular microenvironment *in vivo* affects the variability of reactivity among immune cells. Individual-specific microenvironmental differences play a crucial role in determining macroscopic outcomes, such as the efficacy of immunotherapy and disease progression. The microenvironment is also featured by cytokines released from cells, significantly regulating immune cell function. However, the overall understanding, at single-cell resolution, of how cytokines shape the microenvironment and promote paracrine signaling remains unclear. In this manuscript, we propose a methodology that addresses both the microenvironment itself and the response to the microenvironment to comprehend microenvironment behavior at the single-cell level. Our objective is to contribute to the basic understanding of the interplay between immune cells and their microenvironment, with particular relevance to implications for immunotherapy and disease progression.

KEYWORDS

cytokine, microenvironment, live-cell imaging, heterogeneity, immune response, IFN- β , simulation

1 Introduction

The functions of individual cells are known to exhibit significant variability; however, to maintain a healthy body, it is essential for these cellular functions to be expressed at the appropriate times. The living body possesses mechanisms to ensure the appropriate expression of these cellular functions, one of which involves regulation through the microenvironment formed by the cells themselves (Iwasaki and Medzhitov, 2015; Li et al., 2021). The microenvironment refers to the immediate environment surrounding a particular cell and is formed through the production of signaling molecules such as cytokines and chemokines from the cell. These signaling molecules act on nearby cells and tissues, inducing structural changes such as extracellular matrix remodeling and angiogenesis, as well as attracting additional cells. While the formation of a suitable microenvironment supports the maintenance of health, an unsuitable microenvironment can be detrimental to health. This is especially relevant in immunotherapies that leverage immune cells, where controlling the microenvironment is a key focus for minimizing variability in the target immune cell functions and eliciting specific responses. However,

because signaling molecules are produced in limited quantities and diffuse freely, they are difficult to detect. As a result, the characteristics of the formation process and the dynamics of microenvironments remain poorly understood, making the development of strategies for microenvironment control challenging (Wang et al., 2023; Rosenberg et al., 2008).

In recent years, a range of advanced analytical techniques that retain spatial information have been developed considering the importance of cellular microenvironment. Spatial omics analysis is a method that comprehensively detects gene or protein expression from individual cells within fixed tissue sections (Alexandrov, Saez-Rodriguez, and Saka, 2023). These advancements have been facilitated by the development of various detection technologies, both *in situ* and *ex situ*, as well as by improvements in methods for analyzing spatially structured data, enabling the detection of cell populations with spatially distinctive gene expression patterns (Cui et al., 2024; Singhal et al., 2024). These methods may provide insights into unique cell populations defined by their microenvironment. However, these approaches have limitations as they cannot directly observe the microenvironment itself and only provide snapshot data. This makes it challenging to capture dynamic information, such as changes and developments within the microenvironment.

Flow cytometry analysis using intracellular staining is commonly employed to detect signaling molecules potentially produced by individual cells (Mair and Tosevski, 2014). However, as this method does not retain spatial information, it is inadequate for verifying the microenvironment created by these cells or the microenvironment having influenced these cells, even though it can confirm the presence of specific cytokine-producing cells within a population. Additionally, immunoassays for single-cell analysis, such as ELISPOT and FluoroSpot, are used to detect signaling molecules produced by individual cells (Axelsson, 2022). Nevertheless, these methods do not allow for the simultaneous observation of cells and the signaling molecules they produce, making it challenging to verify whether the produced signaling molecules influence neighboring cells. A method that retains spatial information involves using cells engineered with fluorescent reporter genes for monitoring cytokine expression, which can be effective in imaging studies *in vivo*, tissue sections and *in vitro* model systems (Hwang et al., 2013; Parekh et al., 2024; Scheu, Dresing, and Locksley, 2008). However, this method restricts the types of cytokines that can be analyzed. Additionally, as it detects just the initiation of translation, it does not allow for the observation of cytokine release kinetics. More specifically, it does not necessarily confirm that the cytokines have indeed been released.

This paper focuses on the microenvironment generated when macrophages produce interferon-beta (IFN- β). While the role of IFN- β has been extensively studied in the context of viral infection, it is also recognized for its role in forming critical microenvironments during bacterial infections and cancer immunity (Bogdan, Mattner, and Schleicher, 2004; Decker, Müller, and Stockinger, 2005; Qing and Liu, 2023; Vigo et al., 2019; Cheon, Borden, and Stark, 2014; Yu, Zhu, and Chen, 2022). IFN- β activates innate immune cells, including macrophages, natural killer (NK) cells, and dendritic cells, and promotes the production of chemokines, thereby recruiting other immune cells and amplifying the inflammatory response. Thus, IFN- β is considered a key factor in triggering,

sustaining and advancing immune responses. At the single-cell level, however, there is significant variability in the expression of *Ifnb1*, the gene encoding IFN- β , a phenomenon attributed to the stochastic nature of gene expression (Rand et al., 2012; Zhao et al., 2012). Moreover, several single-cell studies on the response of infected cells have shown that, despite other responses to pathogens, many infected cells do not express *Ifnb1* (Shalek et al., 2014; Patil et al., 2015). The proportion of *Ifnb1*-expressing cells suggests that IFN- β -secreting cells are a minority within the total cell population. This implies the existence of strategies that enable a small number of cells to exert systemic effects (Nandakumar, Windross, and Paludan, 2019; Ji, Shi, and Yin, 2024).

To tackle the challenge of elucidating the precise mechanisms underlying the formation of microenvironments at the single-cell level, we propose an innovative methodology for examining the spatial distribution of IFN- β , encompassing both its presence and effects. We employed an integrated FluoroSpot and RNA-fluorescence *in situ* hybridization (FISH) hybrid assay to visualize IFN- β protein secretion and the response of recipient cells within a population of RAW264.7 mouse macrophage cells stimulated with lipopolysaccharide (LPS). We analyzed microenvironment dynamics using both experimental and simulation data and introduced a novel real-time imaging method, Live Cell Imaging of Secretion Activity (LCI-S) (Shirasaki et al., 2014), to facilitate spatiotemporal evaluation.

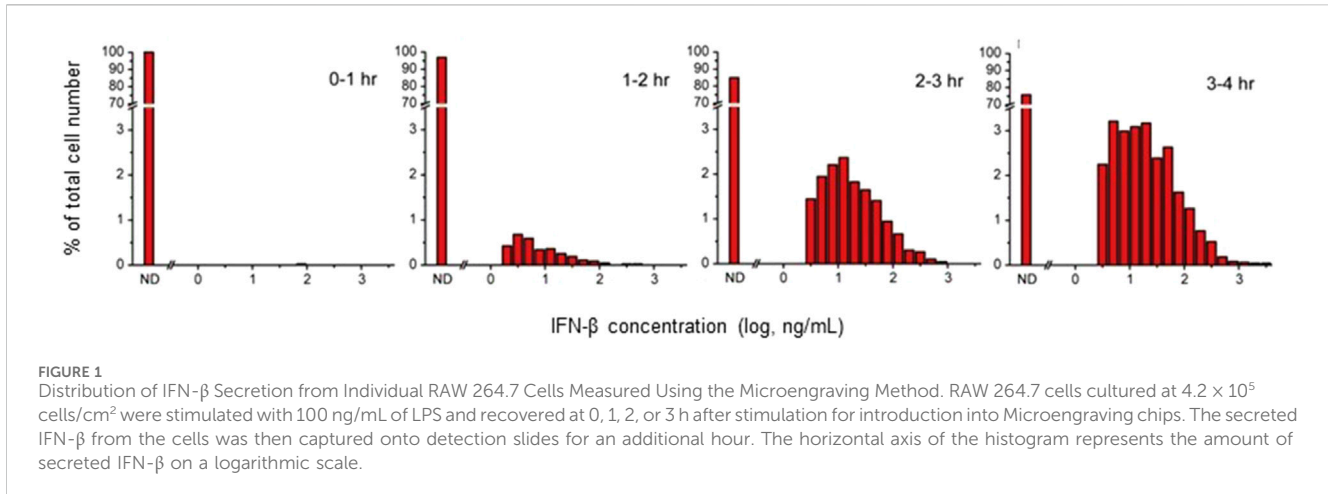
2 Materials and methods

2.1 Cell culture

The murine macrophage cell line RAW 264.7 (ATCC TIB-71) was obtained from the American Type Culture Collection (Manassas, VA, United States) and was maintained in DMEM (08458-45, Nacalai Tesque, Kyoto, Japan) supplemented with 100 U/mL penicillin, 100 μ g/mL streptomycin (26253-84, Nacalai Tesque), and 10% heat-inactivated fetal bovine serum (10437028, Gibco/Thermo Fisher Scientific, Waltham, MA, United States) at 37°C in a humid atmosphere containing 5% CO₂. Cells from passages 5 to 12, following the thawing of the cryostock, were used. In the experiment validating the simulation results, 3 ml of cell suspension was added to each well of a 6-well plate (140675, Nunc/Thermo Fisher Scientific) at the following cell concentrations: Dense: 1.3×10^6 cells/ml, Medium: 1.3×10^5 cells/ml, and Sparse: 1.3×10^4 cells/ml.

2.2 FluoroSpot/RNA-FISH assay

Microscope-grade coverslips were plasma-treated (SEDE-PFA, Meiwafofos) and aminated with Vectabond Reagent (SP-1800, Vector Laboratories). The aminated coverslip was bonded by self-absorption to a polydimethylsiloxane (PDMS) block (Sylgard184, Daw Corning Co.) with a 15-mm-diameter through-hole that served as a cell culture chamber. The glass surface in the chamber was modified with anti-mouse IFN- β antibody (clone# 7F-D3, 7891, Yamasa Corp., Chiba, Japan) using a crosslinker (dimethyl pimelimidate, 21667, Thermo Fisher Scientific) and blocked with monoethanolamine (0.1 M, pH 8.2) and 0.1% Lipidure BL-802 (NOF Corp., Tokyo, Japan). RAW 264.7 cells in a culture dish were



retrieved and diluted in medium at 2.0×10^5 cells/mL. A 400- μ L aliquot of the cell suspension was introduced into the chamber ($=4.5 \times 10^4$ cells/cm²) immediately after administration of 100 ng/mL LPS (Sigma, L6529). Cells in the chamber were incubated for 4 h in a CO₂ incubator at 37°C. After incubation, the cells were washed three times with prewarmed fresh medium and then the F(ab')₂ fragment of anti-mouse IFN- β antibody (0.25 μ g/mL in medium, 32401-1, Pestka Biomedical Laboratories, Inc., Piscataway, NJ, United States) was added. The F(ab')₂ fragment was prepared using a Pierce F(ab')₂ Preparation Kit (44988, Thermo Fisher Scientific). After incubation at 23°C for 20 min, the cells were washed three times with prewarmed fresh medium and stained with Cy3-labeled anti-mouse IgG (30 μ g/mL, 115-165-146, Jackson ImmunoResearch Inc., West Grove, PA, United States). After incubation at 23°C for 20 min, the cells were washed three times with prewarmed fresh medium and fixed in 4% paraformaldehyde (15710, Electron Microscopy Sciences, Hatfield, PA, United States). The fixed cells were subjected to RNA-FISH using the QuantiGene ViewRNA ISH Cell Assay (QVC0001, Affymetrix/Thermo Fisher Scientific) with mouse *Cxcl10*-specific Type 6 probe (Affymetrix ViewRNA probe set, VB6-10663-06) and mouse *Gapdh*-specific Type 4 probe (VB4-10414-06), following the manufacturer's instruction.

Bright-field images and fluorescence images of the cells were acquired with an inverted microscope (ECLIPSE Ti-E, Nikon, Tokyo, Japan) equipped with a $\times 40$ objective (S Fluor $\times 40/0.90$ NA, Nikon), an EM-CCD camera (ImagEM, C9100-13, Hamamatsu Photonics K.K., Shizuoka, Japan), and a high-pressure xenon lamp. In total, 400 areas were scanned for bright-field and three fluorescence images (*Cxcl10*-Alexa 647, *Gapdh*-Alexa 488, and DAPI).

2.3 Image analysis for FluoroSpot/RNA-FISH assay

Images were analyzed using ImageJ (National Institutes of Health). Briefly, background signal obtained by averaging all images followed by median filtering in each color channel was subtracted from every image in each channel. Cell areas were determined by applying edge detection to the bright field, creating binary images, and were segmented by marker-controlled watershed segmentation using DAPI marker images. In *Cxcl10* FISH images with

the background subtracted as described above, the mean fluorescence intensity within each cell area was measured and defined as the *Cxcl10* mRNA expression level. The mean fluorescence intensity around a cell in background-subtracted IFN- β FluoroSpot images was measured as the concentration of IFN- β . The area around the cell was defined as an area where other cells did not overlap in the external 10 pixels ($\approx 3 \mu$ m) of each cell area.

2.4 Mathematical model

2.4.1 Secretion and diffusion of IFN- β

We considered the situation where N cells start secreting IFN- β at some time point within 4 h of LPS stimulation, and the cells are randomly dispersed on a square area with sides of 20 mm at the bottom of the culture dish ($z = 0$). The secreted IFN- β molecules follow Fick's law of diffusion and degrade, with a half-life of 5 h. The spatial dynamics of IFN- β concentration can then be modeled by the following reaction-diffusion equation:

$$\frac{\partial C_{\text{IFN-}\beta}(x, y, z, t)}{\partial t} = -\delta_1 C_{\text{IFN-}\beta}(x, y, z, t) + D \left(\frac{\partial^2 C_{\text{IFN-}\beta}(x, y, z, t)}{\partial x^2} + \frac{\partial^2 C_{\text{IFN-}\beta}(x, y, z, t)}{\partial y^2} + \frac{\partial^2 C_{\text{IFN-}\beta}(x, y, z, t)}{\partial z^2} \right),$$

where $C_{\text{IFN-}\beta}(x, y, z, t)$ is the concentration of IFN- β at position (x, y, z) and time t , and the positive constant δ_1 is the degradation rate of IFN- β . The microengraving results (Figure 1) showed that the fraction of IFN- β -secreting cells gradually increased every hour after LPS stimulation. Although it is not clear whether IFN- β secretion persists for several hours after the start of secretion, the secretion kinetics in this model was simplified as impulse secretion at the onset of secretion. The timing of the pulse secretion from the i -th cell ($i = 1, 2, \dots, N$), say τ_i , was determined by randomly generated numbers with the constraint, which was determined from microengraving results, that 0.08333% of τ_i was distributed between 0 and 60 min, $\Pr(0 \leq \tau_i < 60) = 0.08333 \times 10^{-2}$, and likewise $\Pr(60 \leq \tau_i < 120) = 12.583 \times 10^{-2}$, $\Pr(120 \leq \tau_i < 180) = 71.667 \times 10^{-2}$, and $\Pr(180 \leq \tau_i < 240) = 15.667 \times 10^{-2}$. Using a zero-flux boundary condition at $z = 0$, we solved the reaction-diffusion equation and obtained the analytic form of $C_{\text{IFN-}\beta}(x, y, z, t)$ as:

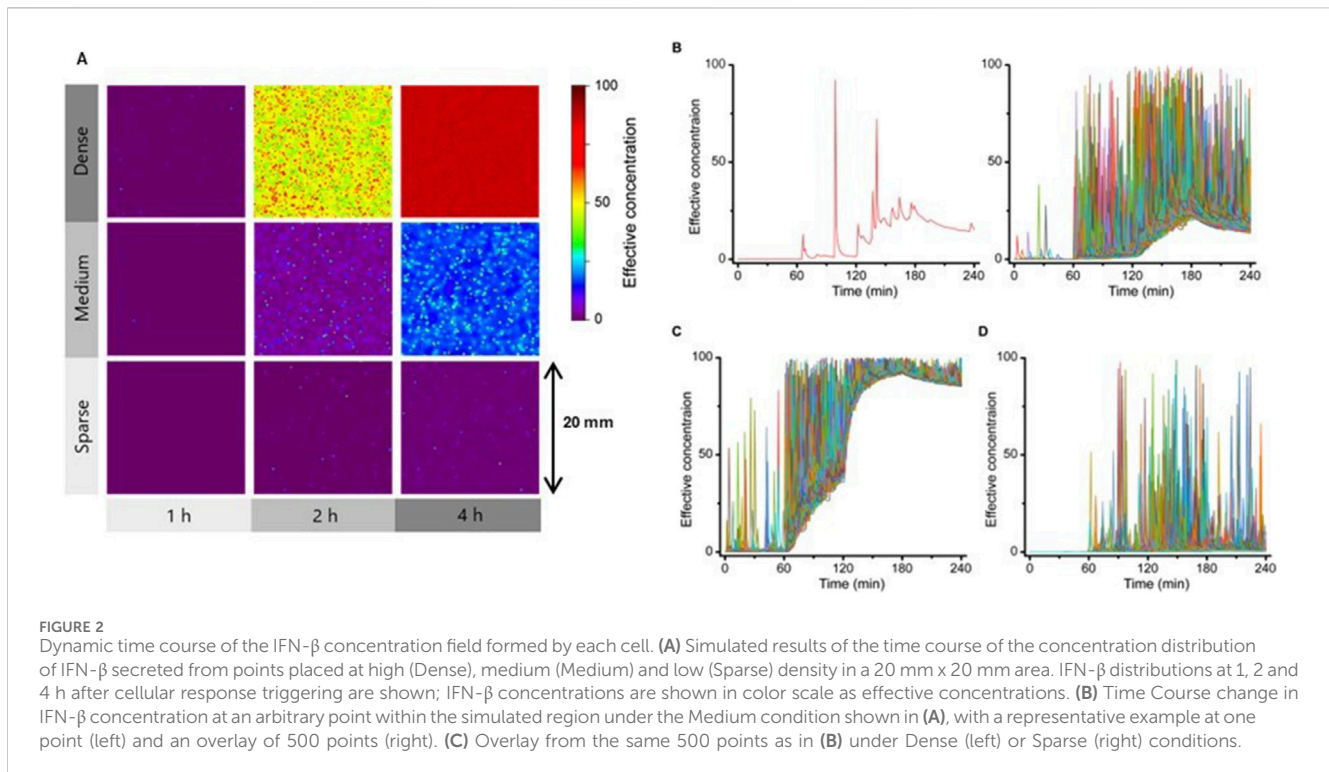


TABLE 1 Parameter values for simulations.

Parameter	Description	Value
δ_1	Degradation rate of IFN-beta	$2.31 \times 10^{-3} \text{ (min}^{-1}\text{)}$
D	Diffusion coefficient of IFN-beta	$6.0 \times 10^{-3} \text{ (mm}^2 \bullet \text{min}^{-1}\text{)}$
G_i	Amount of secreted IFN-beta from each cell	$6.0 \times 10^{-3} \text{ (pg)}$
δ_2	Degradation rate of intermediate molecule	$0.0116 \text{ (min}^{-1}\text{)}$
δ_3	Degradation rate of Cxcl10 mRNA	$0.0116 \text{ (min}^{-1}\text{)}$
β_2	Production rate of intermediate molecule	$8.68 \text{ (copy} \bullet \text{min}^{-1}\text{)}$
β_3	Cxcl10 transcription rate	$37.8 \text{ (copy} \bullet \text{min}^{-1}\text{)}$
γ_2	Hill coefficient for intermediate molecule production	1.00
γ_3	Hill coefficient of Cxcl10 expression	1.53
K_2	Dissociation constant of intermediate molecule production	$76.36 \text{ (pg} \bullet \mu\text{L}^{-1}\text{)}$
K_3	Dissociation constant of Cxcl10 expression	15 (copy)
ϵ_2	Leaky expression rate of intermediate molecule	$2.36 \times 10^{-3} \text{ (copy} \bullet \text{min}^{-1}\text{)}$
ϵ_3	Leaky expression rate of Cxcl10 mRNA	0 (copy \bullet min $^{-1}$)

$$C_{IFN-\beta}(x, y, z, t) = \sum_{i=1}^{N_t} \frac{2G_i}{(4\pi Dt)^{3/2}} \exp(-\delta_1(t - \tau_i)) \frac{\exp(-\frac{(x-x_i)^2 + (y-y_i)^2 + (z-z_i)^2}{4D(t-\tau_i)})}{4D(t-\tau_i)} \quad (1)$$

where (x_i, y_i, z_i) is the position of the i -th cell, and G_i is the amount of IFN- β secreted from the i -th cell. The summation was taken for the cells that secreted IFN- β by time t , and we denoted the number of the secreting cells by N_t . We used this analytic solution to produce

Figure 2A. To simulate Sparse, Medium, and Dense conditions, $N = 10,800, 108,000,$ and $1,080,000$ hypothetical cells were placed within a $30 \text{ mm} \times 30 \text{ mm}$ area, which was equivalent to $12 \text{ cells/mm}^2, 120 \text{ cells/mm}^2,$ and $1,200 \text{ cells/mm}^2,$ respectively. We also considered hypothetical cells located within 5 mm outside of the square area, and simulated secretion of IFN- β to approximate the non-flux boundary at the edge of the square. The secretion timing and the density of the hypothetical cells were set equal to those of the cells inside the square. Other parameter values are summarized in Table 1. The

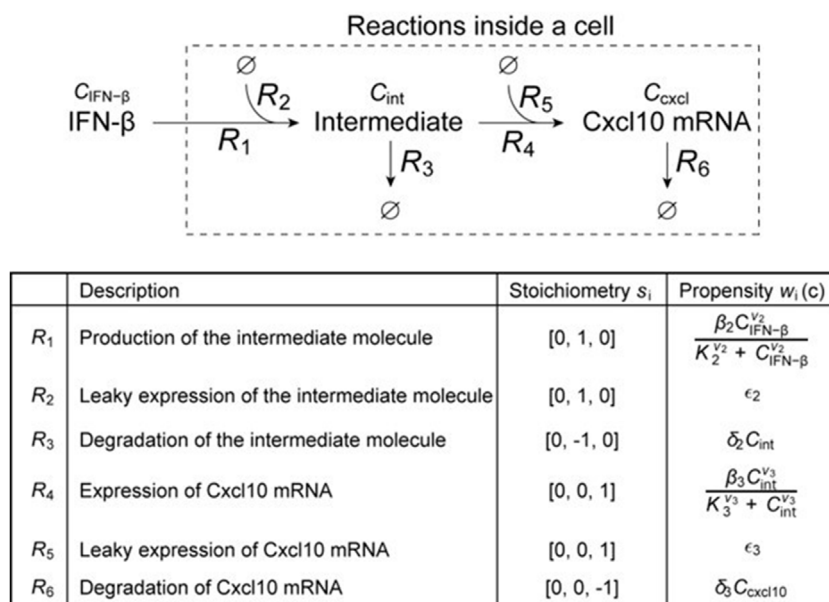


FIGURE 3 Schematic diagram of a simplified model of intracellular signal transduction after the reception of IFN- β , and details of the reactions defined for each route.

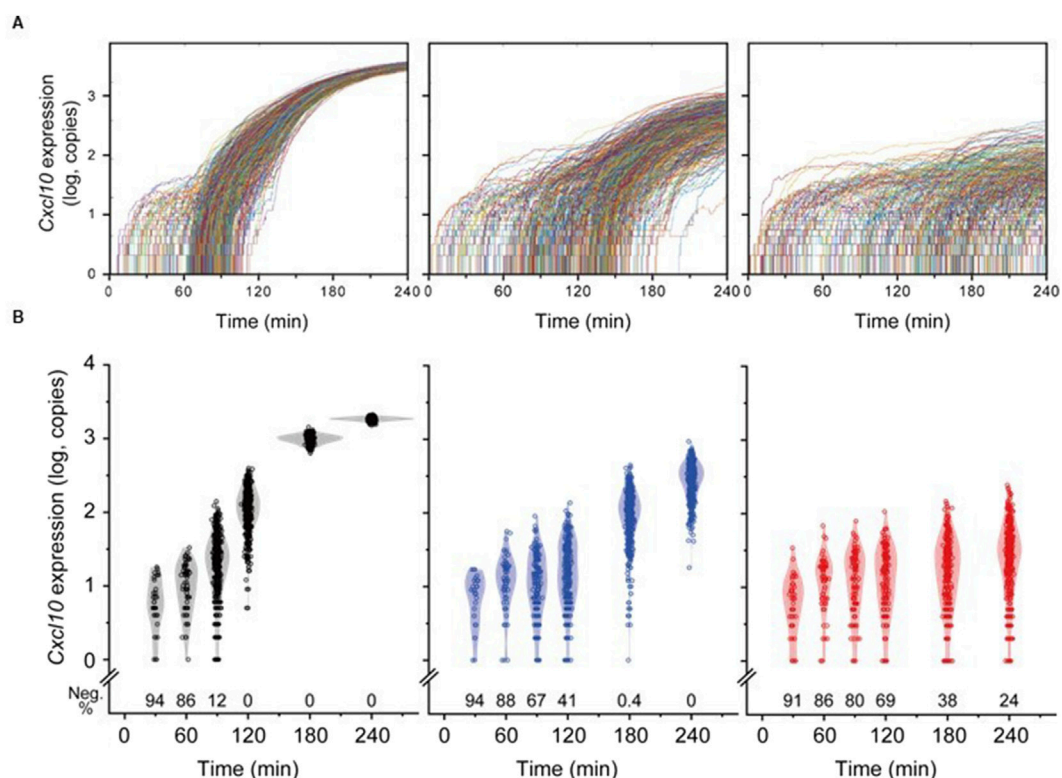


FIGURE 4 Temporal Variation in Individual Cell Responses to the IFN- β Field Generated by Cells. **(A)** Temporal changes in *Cxcl10* expression copy numbers in individual cells. From left to right, corresponding to Dense, Medium, and Sparse conditions, each trace represents data from a single cell. For each cell density condition, traces from 500 cells were overlaid. **(B)** Distribution of responses from all cells in Dense (black), Medium (blue), and Sparse (red). Each dot represents the response level of a single cell, overlaid with a kernel smoothing curve. The bottom of each graph shows the percentage of non-responding cells (Neg.%) at each time point.

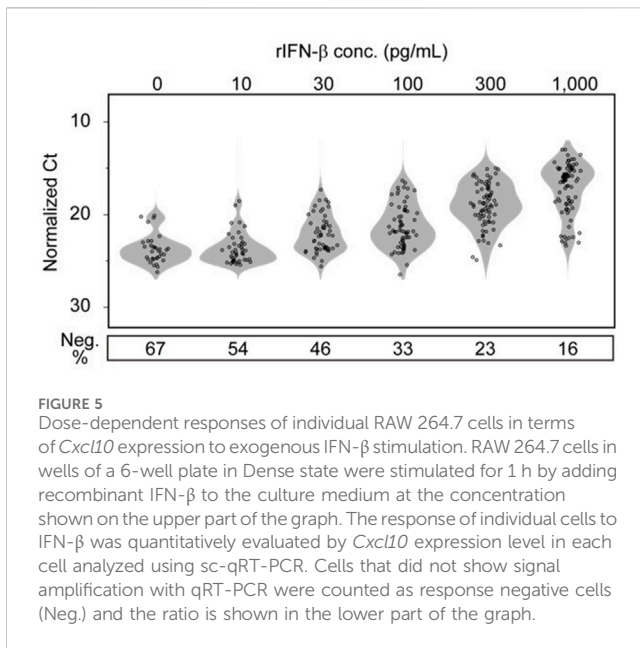


FIGURE 5
Dose-dependent responses of individual RAW 264.7 cells in terms of *Cxcl10* expression to exogenous IFN- β stimulation. RAW 264.7 cells in wells of a 6-well plate in Dense state were stimulated for 1 h by adding recombinant IFN- β to the culture medium at the concentration shown on the upper part of the graph. The response of individual cells to IFN- β was quantitatively evaluated by *Cxcl10* expression level in each cell analyzed using sc-qRT-PCR. Cells that did not show signal amplification with qRT-PCR were counted as response negative cells (Neg.) and the ratio is shown in the lower part of the graph.

diffusion coefficient D was taken as appropriate for the molecular weight of IFN- β and the viscosity of medium containing 10% FBS by estimation according to the Stokes-Einstein equation from the diffusion coefficient of green fluorescent protein (Terada et al., 2005; Swaminathan, Hoang, and Verkman, 1997; Terry, Matthews, and Haseloff, 1995). We assumed that all cells secreted an equal amount of IFN- β ($G_i = 6$ fg for $i = 1, 2, \dots, N$). The simulation codes were implemented and run in MATLAB 2016b.

2.4.2 Stochastic model of *Cxcl10* transcription

We produced a simplified stochastic model that simulates the reception of IFN- β signal and the downstream pathway of *Cxcl10* mRNA transcription. In the model, we reduced the reaction pathways to two steps, as shown in Figure 3. Intermediate molecules between the reception of IFN- β and *Cxcl10* mRNA were reduced to one entity called “Intermediate.” The following stochastic model was obtained based on the chemical master equation (McQuarrie, 1967), which allows for capturing the intrinsic noise due to the low-copy nature of molecules:

$$\frac{\partial \Pr(c, t)}{\partial t} = \sum_{i=1}^6 (w_i(c - s_i) \Pr(c - s_i, t) - w_i(c) \Pr(c, t))$$

where i is the index of reaction specified in Figure 4A, and $c = [C_{\text{IFN-}\beta}, C_{\text{int}}, C_{\text{cxcl}}]$ is the copy number of each molecule as defined in Figure 3. $w_i(\bullet)$ and s_i are the propensity and the stoichiometry of reaction i , respectively (see Figure 3). The parameters were determined as described under Parameter Fitting. The stochastic simulation algorithm (SSA) (Gillespie 1976) was used to simulate the time trajectories in Figure 4A. For each run of the SSA, we simulated the trajectory of a single cell located at the center of a square area of 30 mm \times 30 mm. The extracellular IFN- β concentration at the position of the cell was recalculated for each iteration of the SSA using the reaction-diffusion simulation (Equation (1)), and secretion timings τ_i were resampled. We used 500 cells (500 runs of the SSA)

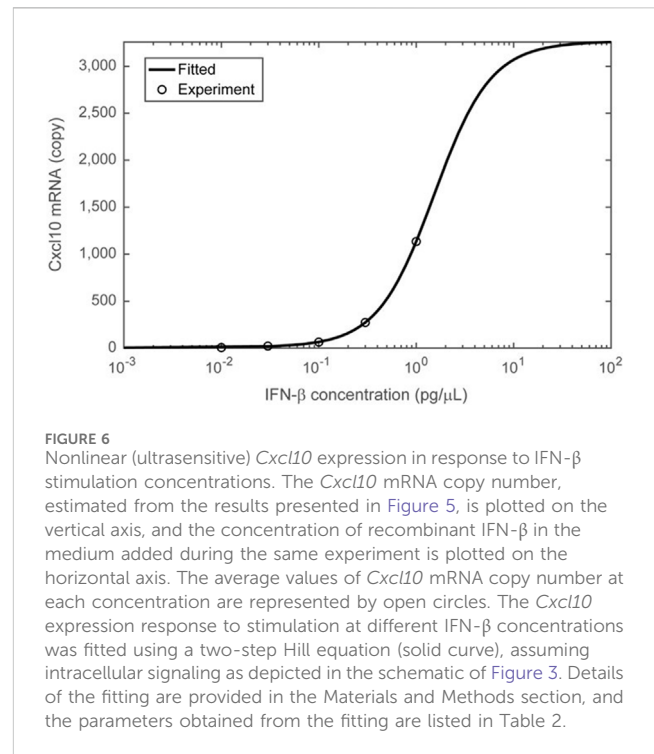


FIGURE 6
Nonlinear (ultrasensitive) *Cxcl10* expression in response to IFN- β stimulation concentrations. The *Cxcl10* mRNA copy number, estimated from the results presented in Figure 5, is plotted on the vertical axis, and the concentration of recombinant IFN- β in the medium added during the same experiment is plotted on the horizontal axis. The average values of *Cxcl10* mRNA copy number at each concentration are represented by open circles. The *Cxcl10* expression response to stimulation at different IFN- β concentrations was fitted using a two-step Hill equation (solid curve), assuming intracellular signaling as depicted in the schematic of Figure 3. Details of the fitting are provided in the Materials and Methods section, and the parameters obtained from the fitting are listed in Table 2.

to plot Figure 4A. All stochastic simulations were conducted in MATLAB 2016b.

2.4.3 Parameter Fitting

To determine the parameters, we used least square fitting to the experimental result of single-cell quantitative real-time polymerase chain reaction (qRT-PCR) for recombinant mouse IFN- β (Figures 5, 6). Specifically, as the Ct value for amplification from one copy was around 26 (data not shown), mean normalized Ct values of the positive samples were converted to the copy number of *Cxcl10* mRNA molecules by $[C_{\text{cxcl}}] = 2^{26 - [\text{normalized Ct}]}$, without amplification efficiency correction. Then, we obtained the parameters by minimizing the square error between $[C_{\text{cxcl}}]$ and C_{cxcl} . We used mass action kinetics and assumed that *Cxcl10* concentration was at steady state to calculate C_{cxcl} . Specifically, C_{cxcl} was calculated by the following formula:

$$C_{\text{int}} = \frac{\gamma_2 [r\text{IFN}]^{\nu_2}}{K_2^{\nu_2} + [r\text{IFN}]^{\nu_2}} + \rho_2$$

$$C_{\text{cxcl}} = \frac{\gamma_3 [C_{\text{int}}]^{\nu_3}}{K_3^{\nu_3} + [C_{\text{int}}]^{\nu_3}} + \rho_3$$

where $\gamma_2 = \beta_2/\delta_2$, $\gamma_3 = \beta_3/\delta_3$, $\rho_2 = \epsilon_2/\delta_2$ and $\rho_3 = \epsilon_3/\delta_3$, and we assumed that the half-life of the intermediate molecule and *Cxcl10* mRNA was 60 min. The fitting result is shown in Figure 6.

2.5 Live cell imaging of secretion activity (LCI-S)

In this study, cells were observed using the method outlined at Transducers 2017 (Tanaka et al., 2017). A custom-made waveguide

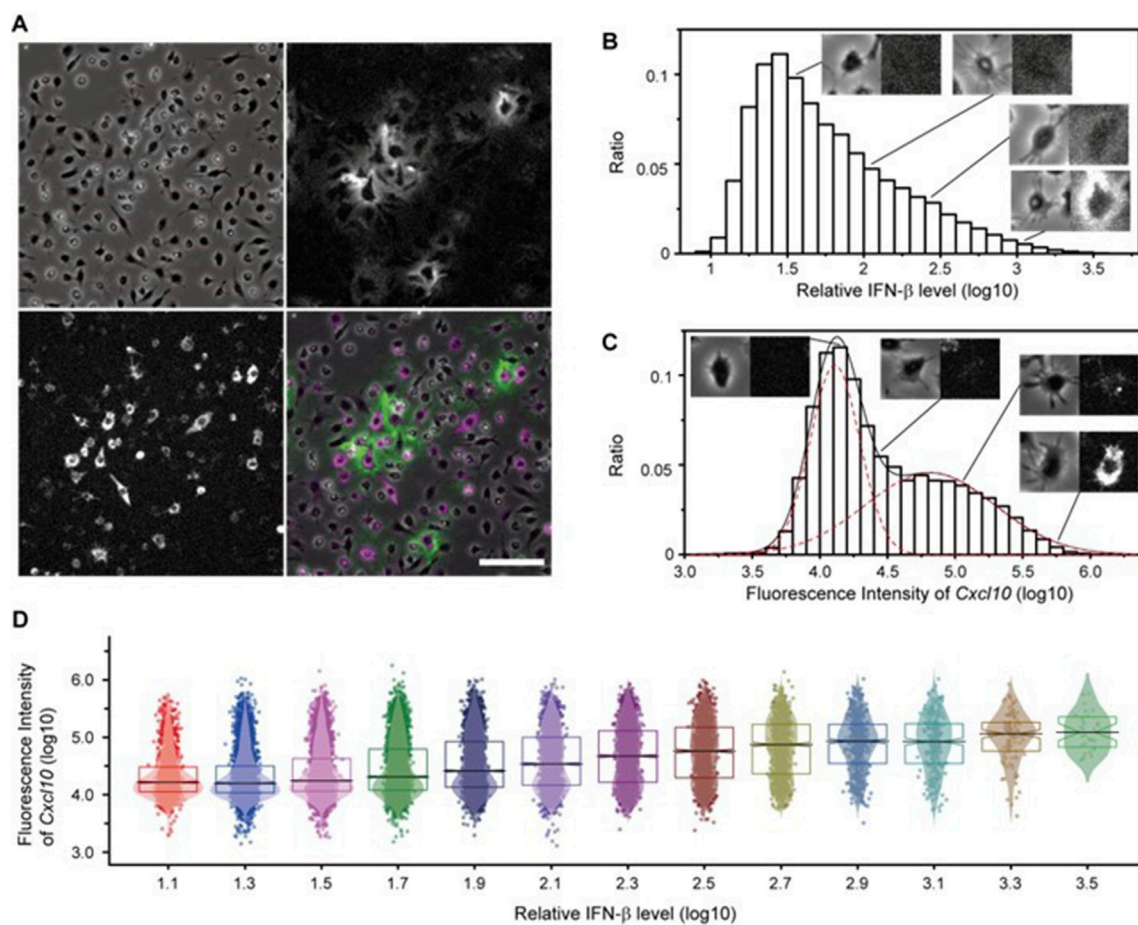


FIGURE 7

Simultaneous Observation of Secreted IFN- β Proteins and Induced Cellular Responses Using the FluoroSpot/RNA-FISH Assay. **(A)** Secreted IFN- β protein (green) visualized by the FluoroSpot assay and *Cxcl10* mRNA expression (magenta) visualized by RNA-FISH after 4 h of stimulation with LPS. Top left: brightfield image; top right: IFN- β ; bottom left: *Cxcl10* mRNA; bottom right: merged image. Scale bar = 100 μ m. **(B)** Distribution of pericellular IFN- β intensity measured from FluoroSpot/RNA-FISH images. Each set of microscopic images (left: bright field; right: IFN- β signal) is shown as a representative cell image at the indicated IFN- β levels. **(C)** Distribution of intracellular *Cxcl10* mRNA intensity measured from FluoroSpot/RNA-FISH images. Each set of microscopic images (left: bright field; right: *Cxcl10* mRNA signal) is shown as a representative cell image at the indicated *Cxcl10* levels. **(D)** Distribution of cellular response per IFN- β level around the cell. Each dot represents the single-cell response level (*Cxcl10* gene expression level), overlaid with a kernel smoothing curve. The black horizontal line represents the median at each IFN- β level, the notch represents the 95% confidence interval around the median, and the boxes represent quartiles.

chip, produced by Live Cell Diagnosis Ltd., was employed to monitor secretion activity during cell culture. The chip has a PDMS cell containment chamber on the top surface of the glass optimized for waveguide optics, and the glass surface was aminated. A mixture of capture antibodies (final concentration of 100 μ g/mL) and dimethyl pimelimidate-2HCl (final concentration of 7 mg/mL) was loaded into the chamber to fix the capture antibodies on the bottom surface. The remaining reaction groups were blocked with monoethanolamine (0.1 M, pH 8.2). The chip with immobilized antibodies was stored in phosphate-buffered saline supplemented with Lipidure BL802 reagent (0.2% w/v) at 4°C until further use.

The biotin-labeled detection antibody was coupled with either CF660R-labeled streptavidin or Cy3-labeled streptavidin at 1:10 molar ratio in the dark for 2 h. Unoccupied sites on streptavidin were blocked with excess dPEG4-biotin acid (10199; Quanta BioDesign, Ltd., Powell, OH, United States). Unconjugated

streptavidin and dPEG4-biotin were removed using ultrafiltration (Amicon Ultra-0.5, 100 kDa; Merck Millipore, Billerica, MA, United States). The detection media containing the prepared CF660R and Cy3-labeled detection antibodies for each antigen were used at a final concentration of 30 nM each.

An aliquot of RAW 264.7 cells was introduced into a chamber of a chip at the frequency of $1.2 \times 10^5/\text{cm}^2$. The culture supernatant was replaced with a freshly prepared detection medium containing 2'3'-Cyclic GMP-AMP (cGAMP) at a final concentration of 50 μ M immediately before observation. The entire area of the chip chamber was scanned every 20 min on the fully automated inverted fluorescence microscopy (Ti2-E, Nikon) with a high numerical (NA=0.95) $\times 20$ objective lens (CFI Apochromat LWD $\times 20$ WI λ S, Nikon), a high-resolution CMOS camera (ORCA-Flash 4.0 v2, Hamamatsu Photonics) and a stage top incubator system (INUBG2TF-WSKM, Tokai Hit), controlled using NIS-Elements software (Nikon).

2.6 Temporal signal deconvolution through image conversion in LCI-S data analysis

The subsequent image analysis method served as a simplified method to estimate secretion activity at a specific time point. Given the frame number at a particular time point as “n,” the average of five consecutive images from “n” to “n+4” was subtracted from the average of five consecutive images from “n-1” to “n-5.” It is important to acknowledge that this method retains a historical context contingent upon the binding speed of the detection antibody.

3 Results

3.1 Visualization of the microenvironment formed by IFN- β utilizing the FluoroSpot/RNA-FISH assay

This study aims to characterize the spatial propagation of functional IFN- β in a model where a specific subset of cells secretes IFN- β within a larger cell population, contributing to microenvironment formation. During the planning stage, we hypothesized that the frequency of IFN- β -producing cells in LPS-stimulated RAW264.7 cells would be moderately low. This assumption was based on the notion that IFN- β production is significantly influenced by the MyD88-dependent pathway. Specifically, the MyD88-independent pathway involved in IFN- β production is activated subsequent to the establishment of the MyD88-dependent pathway, and the IFN- β response is further suppressed by the upregulation of MyD88 (Takeda and Akira, 2004; Kagan et al., 2008; Fitzgerald et al., 2003; Saikh, 2021). Microengraving experiments (Love et al., 2006), outlined in Figure 1, confirmed this hypothesis, showing IFN- β secretion in only a small percentage of cells, reaching only 25% even after 4 h of stimulation.

To assess the microenvironment shaped by IFN- β , we utilized the FluoroSpot/RNA-FISH assay, simultaneously imaging secreted IFN- β and *Cxcl10* mRNA expression. *Cxcl10* is a gene encoding the chemotactic protein interferon γ -induced protein 10 kDa (IP-10), which is known to be induced by IFN. These two elements constitute a minimal model for microenvironment formation, wherein IFN- β released from cells ultimately recruits various immune cells to the local area. This approach demonstrated that highly *Cxcl10* mRNA-expressing cells were frequently observed around substantially IFN- β -secreting cells (Figure 7A). The region where IFN- β was clearly detected was within 50 μ m of secreting cells. Apart from this, a few isolated cells sometimes exhibited elevated *Cxcl10* expression despite low pericellular IFN- β concentrations, suggesting two possible mechanisms: a low-probability induction by background-level IFN- β or direct induction through the MyD88-dependent pathway.

For quantitative evaluation, we measured pericellular IFN- β and intracellular *Cxcl10* signal intensities for each cell, revealing large variability in both (Figures 7B, C). The intensity of the IFN- β signal around cells showed a continuous distribution, indicating not only the presence of a strong IFN- β signal within 50 μ m of the secreting cells but also a theoretically weak, continuous distribution extending indefinitely. In contrast, plotting *Cxcl10* levels on a logarithmic scale revealed two distinct Gaussian peaks, suggesting the coexistence of cells with signals below the

detection limit and a diverse range of expression levels. To determine whether the pericellular IFN- β signal influences *Cxcl10* expression cells were stratified based on the intensity of the pericellular IFN- β the bimodal pattern of *Cxcl10* expression in each stratum exhibited a tendency toward increased median expression as the IFN- β signal intensity rose. Furthermore, the proportion of cells with undetectable *Cxcl10* expression decreased, while the proportion of cells with measurable *Cxcl10* expression increased in regions with higher IFN- β signal intensity (Figure 7D). These findings indicate that the quantified IFN- β signal intensity correlates with the ability of cells to sense IFN- β . Specifically, cells with high peripheral IFN- β signal intensity were predominantly those secreting IFN- β or in close proximity to such cells, and the majority of these cells expressed *Cxcl10*. These results suggest that the *Cxcl10* mRNA response is effectively induced in the microenvironment neighboring IFN- β -secreting cells.

3.2 Simulation of spatial propagation of secreted IFN- β

The FluoroSpot/RNA-FISH system may overestimate the localization of IFN- β concentrations and underestimate baseline elevations because of immobilization of secreted IFN- β . Additionally, the need to detect IFN- β secretion signals around individual cells imposes an upper limit on the permissible cell density. To address these limitations, simulations were employed to investigate whether a microenvironment could form under conditions where IFN- β is allowed to diffuse freely. A mathematical model was created to assess spatial distribution and cell responses. The reaction-diffusion model, simulating IFN- β secretion and diffusion based on Fick's law, utilized parameters from measured data. The simulation results were illustrated as heat maps of IFN- β concentration over time on a 20 mm \times 20 mm open plane (Figure 2A). The secretory cell density in “Medium” condition was set to match that in the FluoroSpot experiment. Additionally, simulations were conducted with a “Dense” condition, representing a 10-fold higher cell density, and a “Sparse” condition, representing a 10-fold lower cell density. Results indicated an overall increase in IFN- β levels in both the “Medium” and “Dense” conditions, with a clear local increase in IFN- β concentration observed near the secreting cells across all density conditions.

To further analyze these dynamics, time-dependent changes in IFN- β concentration at specific spatial points were plotted (Figure 2B). A representative point (left) and superimposed plots from 500 randomly selected points (right) revealed transient peaks in IFN- β concentration, likely resulting from direct secretion events, as well as dynamic changes in the baseline level. Under high-density conditions, the baseline IFN- β level increased significantly (Figure 2C), whereas under low-density conditions, the baseline elevation was minimal (Figure 2D). Collectively, these findings suggest that even when IFN- β diffuses freely, transient local increases in concentration occur depending on secretion rates and distances from secreting cells. Moreover, the baseline IFN- β concentration rises as cell density increases, amplifying the microenvironment's overall signaling capacity. In contrast, at lower cell densities, the baseline increase is minimal, and the frequency of these peaks is notably reduced.

A stochastic model simulated cell responses in the IFN- β field described above, revealing a slower response and a wider distribution of maximum response intensity reached at the 4-h time point under the Sparse condition (Figure 4). While all cells in the Medium condition eventually responded, their maxima remained lower and more diverse compared to Dense conditions. The fact that the microenvironment under Sparse or Medium conditions initiated responses, but could not achieve full activity, suggests the necessity of prolonged exposure situations seen in the Dense condition, such as the baseline increase in IFN- β concentration or high frequency of transient exposure, to elicit full activity. In other words, even when the proportion of IFN- β -producing cells is low, accumulating these cells and increasing their local density can serve as an effective strategy to amplify their impact on surrounding cells. The simulation model suggested that although microenvironments can initiate a response, a single transient exposure to IFN- β may not elicit strong individual cell responses. In the Sparse condition, 76% of cells initiated a response after 4 h. Assuming a correlation between the distance from the secretion point and cellular reactivity, it is suggested that the proximity of IFN- β -secretory cells within a radius of 142 μm , where the area inside the circle centered on the secretion point accounts for 76% of the space, was necessary to initiate a response. Furthermore, given that secretory cells constitute 25% of the total cell population, the average distance between cells was approximately 14 μm under Dense conditions, where a uniform and robust response was observed in all cells. In contrast, under Medium conditions, where all responsive cells exhibited a reaction but with low uniformity, the average distance between cells was approximately 46 μm .

3.3 Comparison of simulation and actual measurements

The subsequent experiment aimed to validate the simulation results of the microenvironment formed by freely diffusing IFN- β (Figure 8). RAW 264.7 cells at different densities (Dense, Medium, and Sparse) were stimulated with LPS for 4 h in conventional cell culture plates, and *Cxcl10* gene expression was quantified by sc-qRT-PCR. Normalizing target gene expression to *Gapdh*, all cells in the Dense condition exhibited high *Cxcl10* expression (60th percentile range 2.54). In the Sparse condition, 27.9% of cells did not express *Cxcl10*, and the Ct value was higher than in the Dense condition (60th percentile range 5.35) indicating a lower expression level. The Medium condition showed intermediate results (60th percentile range 4.18, 15.9% of cells), consistent with simulated outcomes. This confirmed that increasing cell density induces higher and more uniform *Cxcl10* expression through the paracrine effect of IFN- β .

On the other hand, we did not observe differences in expression levels between Medium and Sparse conditions, which did not fully align with the simulation results. The presence of localized cell aggregation, even seen under Sparse condition, suggests that cellular behaviors such as motility may render the microenvironment created by IFN- β -secreting cells more effective compared to simulated scenarios. This contrasts with the simulations, which assumed completely random resting points for cells. Nevertheless, it is essential to consider the contribution of the MyD88-dependent pathway, which directly induces *Cxcl10* expression in LPS-stimulated RAW264.7 cells. To

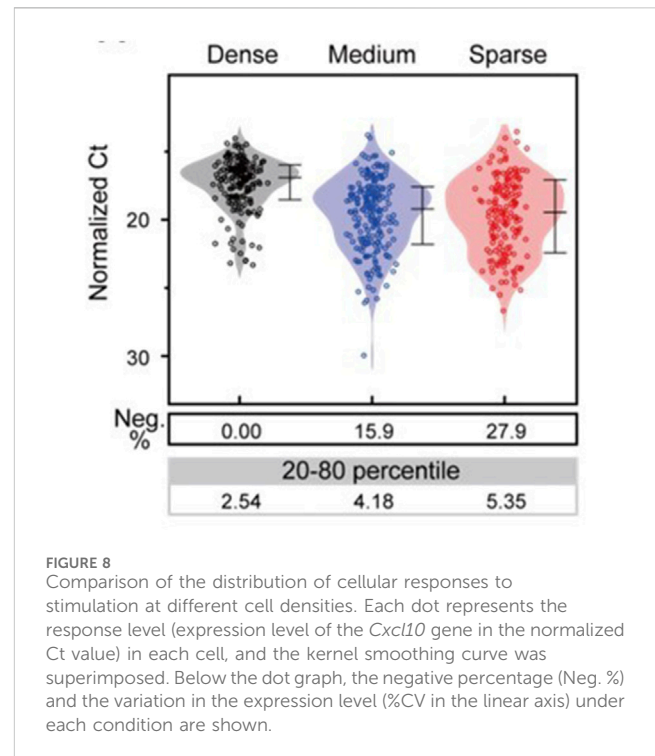


FIGURE 8
Comparison of the distribution of cellular responses to stimulation at different cell densities. Each dot represents the response level (expression level of the *Cxcl10* gene in the normalized Ct value) in each cell, and the kernel smoothing curve was superimposed. Below the dot graph, the negative percentage (Neg. %) and the variation in the expression level (%CV in the linear axis) under each condition are shown.

investigate these hypotheses, we are currently endeavoring to conduct time-lapse imaging studies, as detailed in the following section.

3.4 Visualizing the IFN- β microenvironment with LCI-S

We have the belief that spatiotemporal analysis of cellular responses can provide enhanced insights into the cellular microenvironment. Presently, our investigation is centered on determining whether a time series of responses can be revealed through LCI-S—a real-time secretion visualization method that combines FluoroSpot and total internal reflection fluorescence (TIRF) microscopy. LCI-S employs TIRF microscopy to visualize the FluoroSpot signal of IFN- β to differentiate it from excessive fluorescent antibody without washing processes. This approach allows simultaneous detection of IFN- β release while observing cellular dynamics such as movement and enzymatic activity over time, facilitating the analysis of their relationship. In addition, as a parameter for assessing the impact of the IFN- β microenvironment on cells, the secretion of IP-10, the translation product of *Cxcl10*, was visualized concurrently with the secreted IFN- β . Here, we observed the secretory response of RAW264.7 cells stimulated with cGAMP to avoid complications arising from IFN- β -independent IP-10 secretion via the MyD88-dependent pathway induced by LPS stimulation (see Figure 9 for an example). Following stimulation, IFN- β secretion commenced from certain cells, and subsequently, IP-10 secretion was observed in the surrounding cells. Considering the slow dissociation of the immune complex at the bottom surface, it is reasonable to assume that the observed signal represents cumulative secretory activity.

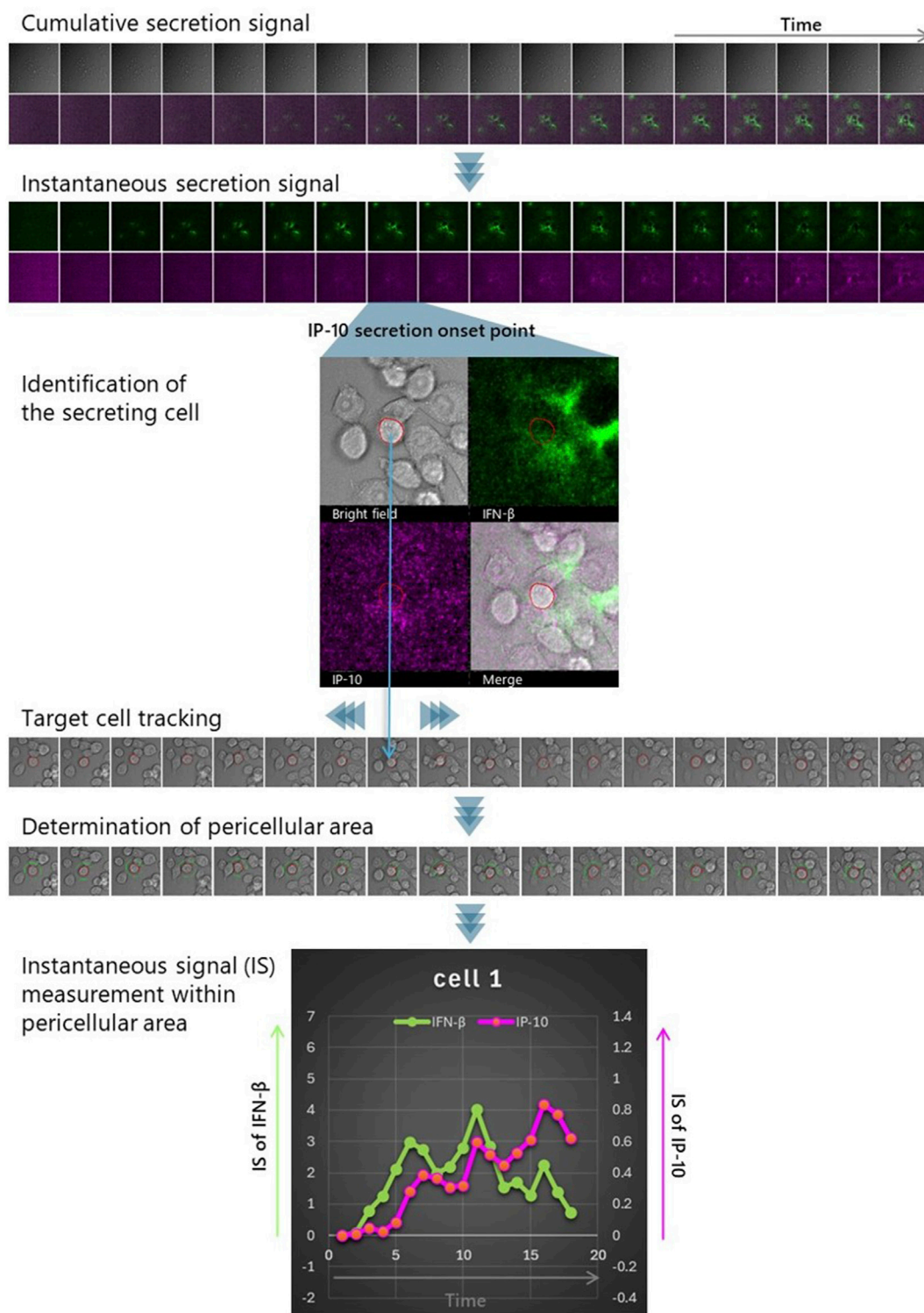


FIGURE 9 Strategies for dynamically detecting interactions with the microenvironment. LCI-S measurements were conducted on RAW264.7 cells cultured at a density of 1×10^5 cells/cm² on a TIRF chip. Immediately before starting observation, the culture medium was supplemented with 50 μ M cGAMP and detection antibodies for IFN- β and IP-10, labeled with distinct dyes. Time-lapse imaging was performed every 20 min, capturing bright-field images along with IFN- β (green) and IP-10 (magenta) signals (*Cumulative secretion signal*). Subsequently, after reducing noise by rolling average for 5 frames, difference images were generated from each pair of consecutive images in the time series (*Instantaneous secretion signal*). Based on these difference images, cells that initiated IP-10 secretion were detected (*Identification of the secreting cell*), and their movement was tracked using the bright-field images before and after (*Target cell tracking*). The outlines of the tracked cells at each time point were extracted, and an extended region 3 μ m beyond the cell perimeter was defined as the pericellular area (*Determination of pericellular area*). By measuring changes in the intensity of IFN- β and IP-10 signals (Continued)

FIGURE 9 (Continued)

within this pericellular area, the exposure history of IP-10-secreting cells to IFN- β can be determined. This allows for the evaluation of the IFN- β microenvironment's influence on IP-10 secretion, including the intensity and timing of the response (*Instantaneous signal (IS) measurement within the pericellular area*).

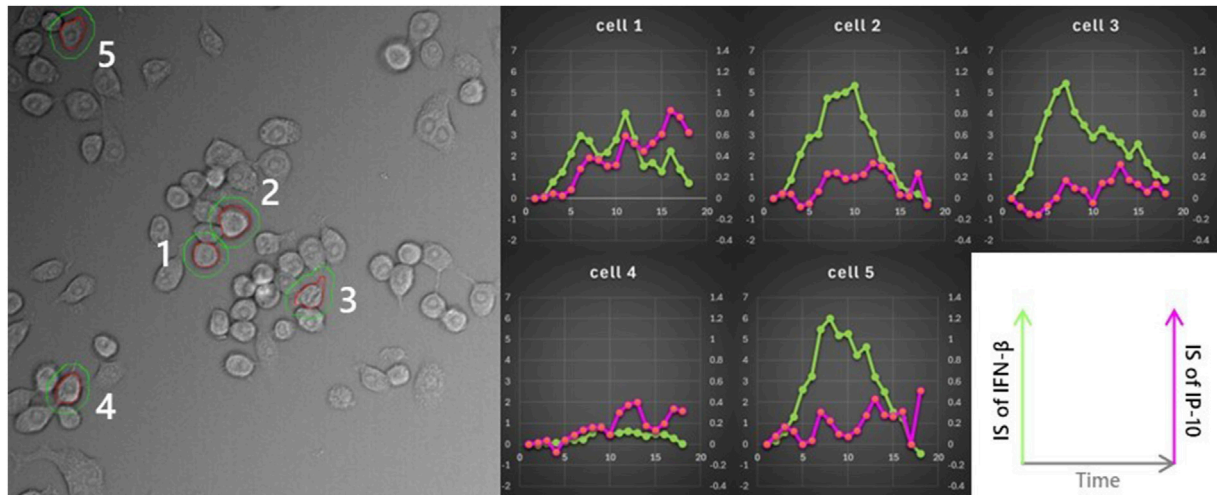


FIGURE 10

Association between the IFN- β microenvironment perceived by cells and IP-10 secretion. The same analysis was applied to five cells in the same field of view, following the strategy outlined in Figure 9. All cells, except for cell 4, were exposed to high concentrations of IFN- β . However, cell 4 did not exhibit any clear interaction with the microenvironment.

Since the cumulative secretory activity signal represents IFN- β rendered non-functional due to immobilization, we chose to apply basic image processing techniques to isolate the moment of secretion, when functional IFN- β is presumed to be most abundant, and interpret this isolated signal as the functional IFN- β microenvironment (see Methods for details).

The correlation between IP-10 secretion and exposure to active IFN- β was assessed by overlaying the positional history of IP-10-secreting cells onto the calculated IFN- β instantaneous secretion images. We quantified and graphically represented the pericellular IFN- β and IP-10 instantaneous secretion of IP-10 secreting cells, respectively (see Figure 9). This analysis was replicated for the five cells presented, and the resultant changes in pericellular IFN- β and IP-10 signal intensity are illustrated in Figure 10. Notably, in four out of the five cells, a substantial increase in IFN- β signal was observed, preceding the rise in IP-10 secretory signal.

Thus, time-course measurements using LCI-S present a unique method for monitoring dynamic cell-cell interactions mediated by cytokines and elucidating causal relationships. We propose this as an innovative approach to understand the dynamic nature of cellular microenvironments.

4 Discussion

In this paper, we have examined methodologies aimed at elucidating both the microenvironment itself and cellular responses to it, with the goal of advancing the understanding of cellular microenvironments. The analytical approach that preserves

spatial information aligns with the principles of spatial omics analysis (Alexandrov, Saez-Rodriguez, and Saka, 2023); however, it differs in that it enables the spatial discussion of causality between locally distinctive cell populations and microenvironment-forming cytokines that may drive the formation of such populations.

First, we underscored the significance of analyses that retain spatial context, exemplified by the FluoroSpot/RNA-FISH assay. Under the conditions applied in this study, the microenvironment created by an individual cell was detectable within a radius of approximately 50 μm . While the *Cxcl10* expression response was pronounced within this range, its efficiency declined at greater distances. These findings do not suggest that the minority of IFN- β -producing cells enhanced the activity of the whole cells in the population. This observation is likely attributable to a combination of factors: the decrease in IFN- β concentration as it diffuses three-dimensionally away from the secreting cell, and the ultrasensitivity of cells to IFN- β . However, due to the immobilization of antibodies in the FluoroSpot setup for capturing target signal molecules, there was a potential risk of underestimating the diffusion range and impact of these molecules on cells.

To address this, we integrated single-cell measurements with numerical simulations to gain insights into the microenvironment formed by IFN- β -producing cells. Simulations offer robust solutions to compensate for the compromises made when visualizing certain physical quantities. Nonetheless, it is crucial to recognize that simulations can potentially overestimate or underestimate biological parameters that are not considered, necessitating the acquisition and comparison of real measurements under conditions that closely replicate the simulated setup. Experiments using simulations and actual cell cultures at three

different densities demonstrated that when cells were cultured at high density, *Cxcl10* mRNA expression was uniformly induced across the cell population, with consistently high expression levels and minimal variability. The strong and uniform response was attributed to either an increased peak frequency, a higher background level, or a combination of both. This suggests that even without an increase in the proportion of IFN- β -secreting cells, the IFN- β microenvironment can effectively influence the entire cell population through localized accumulation.

We subsequently presented a live-cell imaging approach to elucidate the dynamic changes in the microenvironment induced by active cells movements. This method involves spatiotemporal analysis, offering a comprehensive examination that considers cellular secretory functions, motility, and other dynamic properties.

A crucial aspect of the proposed method is the conversion of cumulative signals of secretory activity into instantaneous signals. Simulation of cytokine kinetics motivated us to develop the method. An image analysis method for this conversion, based on the law of mass action, is currently under development and will be presented shortly.

In conclusion, by visualizing the cellular microenvironment using fluorescence live-cell imaging and validating these findings through simulations, we have uncovered how a small subset of cells secreting signaling molecules can create a microenvironment capable of influencing the entire cell population. Our model demonstrates that while signaling molecules secreted by individual cells create a highly localized microenvironment, increasing the frequency of signaling cells through localized cell accumulation effectively activates the entire population. It is well established that various chemokines promote cell localization (Weninger et al., 2014; Natsuaki et al., 2014; Brewitz et al., 2017; Kienle et al., 2021; Khazen et al., 2022). Additionally, recent single-cell secretion analyses have revealed that, in many cell types, only a small fraction of the population exhibits the expected secretion activity (Bucheli et al., 2021; Yamagishi et al., 2024). This low frequency of secretion may be advantageous for the body, as it can serve as a safety mechanism to prevent excessive signal transduction when combined with processes such as chemotaxis and cell aggregation.

Advances in single-cell biology have enabled the acquisition of detailed information at the single-cell level. The future challenge lies in elucidating the principles governing the interactions between the microenvironment and individual cells at the single-cell level. This kind of dynamic analysis including simulations and time-lapse measurements will identify new parameters regulating microenvironment efficacy, which promises to contribute to future medical advancements, such as improvements in cell-based therapies and immunotherapy.

Data availability statement

The raw data supporting the conclusions of this article will be made available by the authors, without undue reservation.

Ethics statement

Ethical approval was not required for the studies on animals in accordance with the local legislation and institutional

requirements because only commercially available established cell lines were used.

Author contributions

MY: Conceptualization, Data curation, Formal Analysis, Funding acquisition, Investigation, Methodology, Validation, Visualization, Writing—original draft, Writing—review and editing. YuH: Data curation, Formal Analysis, Investigation, Methodology, Software, Visualization, Writing—original draft, Writing—review and editing. NS: Investigation, Writing—review and editing. YP: Investigation, Writing—review and editing. YoH: Project administration, Writing—review and editing. TF: Project administration, Writing—review and editing. OO: Project administration, Supervision, Writing—review and editing. YS: Conceptualization, Funding acquisition, Methodology, Project administration, Supervision, Writing—review and editing.

Funding

The author(s) declare that financial support was received for the research, authorship, and/or publication of this article. This work was supported by the Naito Foundation (to MY) and partially by Japan Science and Technology Agency (JST), Precursory Research for Embryonic Science and Technology (PRESTO) (Grant Number JP17940748), and JST Moonshot R&D (Grant Number JPMJMS2217-4-2) (to YS).

Acknowledgments

The authors thank the FACS Lab in RCAI (now IMS) of RIKEN for technical assistance on FACS experiments. We thank Tomohiko Okazaki for incisive comments.

Conflict of interest

Authors MY and NS were employed by Live Cell Diagnosis, Ltd.

The remaining authors declare that the research was conducted in the absence of any commercial or financial relationships that could be construed as a potential conflict of interest.

Publisher's note

All claims expressed in this article are solely those of the authors and do not necessarily represent those of their affiliated organizations, or those of the publisher, the editors and the reviewers. Any product that may be evaluated in this article, or claim that may be made by its manufacturer, is not guaranteed or endorsed by the publisher.

References

- Alexandrov, T., Saez Rodriguez, J., and Saka, S. K. (2023). Enablers and challenges of spatial omics, a melting pot of technologies. *Mol. Syst. Biol.* 19 (11), e10571. doi:10.15252/msb.202110571
- Axelsson, B. (2022). Detection and enumeration of cytokine-secreting cells by FluoroSpot. *Methods Mol. Biol.* 2386, 81–99. doi:10.1007/978-1-0716-1771-7_6
- Brewitz, A., Eickhoff, S., Dähling, S., Quast, T., Bedoui, S., Kroczeck, R. A., et al. (2017). CD8+ T cells orchestrate PDC-XCR1+ dendritic cell spatial and functional cooperativity to optimize priming. *Immunity* 46 (2), 205–19. doi:10.1016/j.immuni.2017.01.003/ATTACHMENT/4CEDBF7B-22CC-47F2-8B69-28BFAED3D53B/MMC10.PDF
- Bogdan, C., Mattner, J., and Schleicher, U. (2004). The role of type I interferons in non-viral infections. *Immunol. Rev.* 202 (1), 33–48. doi:10.1111/j.0105-2896.2004.00207.x
- Bucheli, O. T. M., Sigvaldadóttir, L., and Eyer, K. (2021). Measuring single-cell protein secretion in immunology: technologies, advances, and applications. *Eur. J. Immunol.* 51 (6), 1334–47. doi:10.1002/eji.202048976
- Cheon, H., Borden, E. C., and Stark, G. R. (2014). Interferons and their stimulated genes in the tumor microenvironment. *Seminars Oncol.* 41 (2), 156–173. doi:10.1053/j.seminoncol.2014.02.002
- Cui, T., Li, Y. Y., Li, B.-L., Zhang, H., Yu, T.-T., Zhang, J.-N., et al. (2024). SpatialRef: a reference of spatial omics with known spot annotation. *Nucleic Acids Res.* 1 (1256879), gkae892–14. doi:10.1093/NAR/GKAE892
- Decker, T., Müller, M., and Stockinger, S. (2005). The Yin and yang of type I interferon activity in bacterial infection. *Nat. Rev. Immunol.* 5 (9), 675–687. doi:10.1038/nri1684
- Fitzgerald, K. A., Rowe, D. C., Barnes, B. J., Caffrey, D. R., Visintin, A., Latz, E., et al. (2003). LPS-TLR4 signaling to IRF-3/7 and NF- κ B involves the toll adapters TRAM and TRIF. *J. Exp. Med.* 198 (7), 1043–1055. doi:10.1084/JEM.20031023
- Gillespie, D. T. (1976). A general method for numerically simulating the stochastic time evolution of coupled chemical reactions. *J. Comput. Phys.* 22 (4), 403–434. doi:10.1016/0021-9991(76)90041-3
- Hwang, S.-Y., Hur, K.-Y., Kim, J.-R., Cho, K.-H., Kim, S.-H., and Yoo, J.-Y. (2013). Biphasic RLR-IFN- β response controls the balance between antiviral immunity and cell damage. *J. Immunol.* 190 (3), 1192–1200. doi:10.4049/JIMMUNOL.1202326
- Iwasaki, A., and Medzhitov, R. (2015). Control of adaptive immunity by the innate immune system. *Nat. Immunol.* 16 (4), 343–353. doi:10.1038/ni.3123
- Ji, S., Shi, Y., and Yin, B. (2024). Macrophage barrier in the tumor microenvironment and potential clinical applications. *Cell. Commun. Signal.* 22 (1), 74–14. doi:10.1186/S12964-023-01424-6
- Kagan, J. C., Su, T., Horng, T., Chow, A., Akira, S., and Medzhitov, R. (2008). TRAM couples endocytosis of Toll-like receptor 4 to the induction of interferon- β . *Nat. Immunol.* 9, 361–368. doi:10.1038/ni1569
- Khazen, R., Corre, B., Garcia, Z., Lemaitre, F., Bachelier-Bassi, S., d'Enfert, C., et al. (2022). "Spatiotemporal Dynamics of Calcium Signals during Neutrophil Cluster Formation", in *Proceedings of the National Academy of Sciences of the United States of America* 119 (29), e2203855119. doi:10.1073/PNAS.2203855119/SUPPL_FILE/PNAS.2203855119.SM11.AVI
- Kienle, K., Glaser, K. M., Eickhoff, S., Mihlan, M., Knöpper, K., Reátegui, E., et al. (2021). Neutrophils self-limit swarming to contain bacterial growth in vivo. *Science* 372 (6548). doi:10.1126/SCIENCE.ABE7729/SUPPL_FILE/ABE7729_KIENLE_SM.PDF
- Li, X., Shao, M., Zeng, X., Qian, P., and Huang, H. (2021). Signaling pathways in the regulation of cytokine release syndrome in human diseases and intervention therapy. *Signal Transduct. Target. Ther.* 6, 367. doi:10.1038/s41392-021-00764-4
- Love, J. C., Ronan, J. L., Grotenbreg, G. M., Van Der Veen, A. G., and Ploegh, H. L. (2006). A microengraving method for rapid selection of single cells producing antigen-specific antibodies. *Nat. Biotechnol.* 24 (6), 703–707. doi:10.1038/nbt1210
- Mair, F., and Tosevski, V. (2014). Intracellular staining for cytokines and transcription factors. *Methods Mol. Biol.* 1193, 39–49. doi:10.1007/978-1-4939-1212-4_5
- McQuarrie, D. A. (1967). Stochastic approach to chemical kinetics. *J. Appl. Probab.* 4 (3), 413–478. doi:10.2307/3212214
- Nandakumar, R., Windross, S. J., and Paludan, S. R. (2019). Intercellular communication in the innate immune system through the CGAS-STING pathway. *Methods Enzym.* 625, 1–11. doi:10.1016/bs.mie.2019.07.007
- Natsuaki, Y., Egawa, G., Nakamizo, S., Ono, S., Hanakawa, S., Okada, T., et al. (2014). Perivascular leukocyte clusters are essential for efficient activation of effector t cells in the skin. *Nat. Immunol.* 15 (11), 1064–69. doi:10.1038/ni.2992
- Parekh, N. J., Winship, D., Van Dis, E., and Stetson, D. B. (2024). Regulation and dynamics of IFN- β expression revealed with a knockin reporter mouse. *J. Immunol.* j2400227. doi:10.4049/JIMMUNOL.2400227
- Patil, S., Fribourg, M., Ge, Y., Batish, M., Tyagi, S., Hayot, F., et al. (2015). Single-cell analysis shows that paracrine signaling by first responder cells shapes the interferon- β response to viral infection. *Sci. Signal.* 8 (363), ra16. doi:10.1126/scisignal.2005728
- Qing, F., and Liu, Z. (2023). Interferon regulatory factor 7 in inflammation, cancer and infection. *Front. Immunol.* 14, 1190841. doi:10.3389/fimmu.2023.1190841
- Rand, U., Rinas, M., Schwerk, J., Nöhren, G., Linnes, M., Kröger, A., et al. (2012). Multi-layered stochasticity and paracrine signal propagation shape the type-I interferon response. *Mol. Syst. Biol.* 8 (May), 584. doi:10.1038/msb.2012.17
- Rosenberg, S. A., Restifo, N. P., Yang, J. C., Morgan, R. A., and Dudley, M. E. (2008). Adoptive cell transfer: a clinical path to effective cancer immunotherapy. *Nat. Rev. Cancer* 8, 299–308. doi:10.1038/nrc2355
- Saikh, K. U. (2021). MyD88 and beyond: a perspective on MyD88-targeted therapeutic approach for modulation of host immunity. *Immunol. Res.* 69 (2), 117–128. doi:10.1007/s12026-021-09188-2
- Scheu, S., Dresing, P., and Locksley, R. M. (2008). Visualization of IFN β production by plasmacytoid versus conventional dendritic cells under specific stimulation conditions in vivo. *Proc. Natl. Acad. Sci.* 105 (51), 20416–20421. doi:10.1073/pnas.0808537105
- Shalek, A. K., Satija, R., Shuga, J., Trombetta, J. J., Gennert, D., Lu, D., et al. (2014). Single-cell RNA-seq reveals dynamic paracrine control of cellular variation. *Nature* 510, 363–369. doi:10.1038/nature13437
- Shirasaki, Y., Yamagishi, M., Suzuki, N., Izawa, K., Nakahara, A., Mizuno, J., et al. (2014). Real-time single-cell imaging of protein secretion. *Sci. Rep.* 4 (1), 4736. doi:10.1038/srep04736
- Singhal, V., Chou, N., Lee, J., Yue, Y., Liu, J., Chock, W. K., et al. (2024). BANKSY unifies cell typing and tissue domain segmentation for scalable spatial omics data analysis. *Nat. Genet.* 56, 431–441. doi:10.1038/s41588-024-01664-3
- Swaminathan, R., Hoang, C. P., and Verkman, A. S. (1997). Photobleaching recovery and anisotropy decay of green fluorescent protein GFP-S65T in solution and cells: cytoplasmic viscosity probed by green fluorescent protein translational and rotational diffusion. *Biophysical J.* 72 (4), 1900–1907. doi:10.1016/S0006-3495(97)78835-0
- Takeda, K., and Akira, S. (2004). TLR signaling pathways. *Seminars Immunol.* 16 (1), 3–9. doi:10.1016/j.smim.2003.10.003
- Tanaka, Y., Suzuki, N., Mora, K., Mizuno, J., Shoji, S., Uemura, S., et al. (2017). "Widefield real-time single-cell secretion imaging with optical waveguide technique," in *Transducers 2017 - 19th international conference on solid-state sensors, actuators and microsystems*. doi:10.1109/TRANSDUCERS.2017.7994363
- Terada, N., Tadakuma, H., Ishihama, Y., Yamagishi, M., Zako, T., and Funatsu, T. (2005). Analysis of nuclear microenvironments by translational diffusion of GFP using fluorescence correlation spectroscopy. *Bioimages* 13, 1–10. doi:10.11169/bioimages.13.1
- Terry, B. R., Matthews, E. K., and Haseloff, J. (1995). Molecular characterization of recombinant green fluorescent protein by fluorescence correlation microscopy. *Biochem. Biophysical Res. Commun.* 217 (1), 21–27. doi:10.1006/BBRC.1995.2740
- Vigo, T., La Rocca, C., Faicchia, D., Procaccini, C., Ruggieri, M., Salvetti, M., et al. (2019). IFN β enhances mesenchymal stromal (Stem) cells immunomodulatory function through STAT1-3 activation and mTOR-associated promotion of glucose metabolism. *Cell. Death and Dis.* 10 (2), 85. doi:10.1038/s41419-019-1336-4
- Wang, Q., Shao, X., Zhang, Y., Zhu, M., Wang, F. X. C., Mu, J., et al. (2023). Role of tumor microenvironment in cancer progression and therapeutic strategy. *Cancer Med.* 12, 11149–11165. doi:10.1002/cam4.5698
- Weninger, W., Biro, M., and Jain, R. (2014). Leukocyte migration in the interstitial space of non-lymphoid organs. *Nat. Rev. Immunol.* 14 (4), 232–46. doi:10.1038/nri3641
- Yamagishi, M., Miyata, K., Kamatani, T., Kabata, H., Baba, R., Tanaka, Y., et al. (2024). Quantitative live-cell imaging of secretion activity reveals dynamic immune responses. *IScience* 27 (6). doi:10.1016/j.isci.2024.109840
- Yu, R., Zhu, B., and Chen, D. (2022). Type I interferon-mediated tumor immunity and its role in immunotherapy. *Cell. Mol. Life Sci.* 79, 191. doi:10.1007/s00018-022-04219-z
- Zhao, M., Zhang, J., Phatnani, H., Scheu, S., and Maniatis, T. (2012). Stochastic expression of the interferon- β gene. *PLOS Biol.* 10 (1), e1001249. doi:10.1371/JOURNAL.PBIO.1001249